Calculating track thrust with track functions

Hsi-Ming Chang,[1] Massimiliano Procura,[2] Jesse Thaler,[3] and Wouter J. Waalewijn[1]

[1]*Department of Physics, University of California at San Diego, La Jolla, California 92093, USA*
[2]*Albert Einstein Center for Fundamental Physics, Institute for Theoretical Physics, University of Bern, CH-3012 Bern, Switzerland*
[3]*Center for Theoretical Physics, Massachusetts Institute of Technology, Cambridge, Massachusetts 02139, USA*
(Received 7 July 2013; published 27 August 2013)

In e^+e^- event shapes studies at LEP, two different measurements were sometimes performed: a "calorimetric" measurement using both charged and neutral particles and a "track-based" measurement using just charged particles. Whereas calorimetric measurements are infrared and collinear safe, and therefore calculable in perturbative QCD, track-based measurements necessarily depend on nonperturbative hadronization effects. On the other hand, track-based measurements typically have smaller experimental uncertainties. In this paper, we present the first calculation of the event shape "track thrust" and compare to measurements performed at ALEPH and DELPHI. This calculation is made possible through the recently developed formalism of track functions, which are nonperturbative objects describing how energetic partons fragment into charged hadrons. By incorporating track functions into soft-collinear effective theory, we calculate the distribution for track thrust with next-to-leading logarithmic resummation. Due to a partial cancellation between nonperturbative parameters, the distributions for calorimeter thrust and track thrust are remarkably similar, a feature also seen in LEP data.

I. INTRODUCTION

Detailed investigations of hadronic final states are crucial for understanding the dynamics of high-energy particle collisions. Charged particles play a particularly important role in these investigations. Whereas neutral particles can only be measured using calorimetry, charged particles can also be measured using tracking detectors, which allows for excellent momentum resolution and vertex identification. At colliders like LEP, tracks were used to perform precision tests of quantum chromodynamics (QCD) through measurements of e^+e^- event shapes and N-jet production rates [1,2] (see Refs. [3–7] for reviews). These LEP studies also tested hadronization models through measurements of charged hadron inclusive distributions. Presently at the LHC, tracking information is used to improve jet measurements, to understand jet substructure, and to mitigate the effects of multiple "pileup" collisions per single bunch crossing.

Despite the experimental advantages offered by tracks, most experimental and theoretical studies are aimed at infrared and collinear- (IRC-) safe observables, which include contributions from both neutral and charged particles. In contrast, there are comparatively few theoretical tools available to understand and predict track-based observables. While fragmentation functions (FFs) are useful for understanding the distribution of single charged particles, more general observables require nonperturbative information about charged particle correlations. For example, Refs. [8,9] showed how new nonperturbative functions are needed to calculate the energy-weighted charge of a jet. Recently in Ref. [10], we introduced the formalism of track functions, which enables QCD

calculations to be performed on a broad class of track-based observables, where (otherwise) IRC-safe observables are modified to include only charged particles.

In this paper, we show how to use track functions to calculate track-based e^+e^- event shapes in perturbative QCD. The track function $T_i(x, \mu)$ is a nonperturbative object that describes how an energetic parton i fragments to a collection of tracks carrying a fraction x of the original parton energy [10]. Like the FF and the jet charge distribution, the track function has a well-defined renormalization group (RG) evolution in μ, such that one can measure $T_i(x, \mu)$ at one scale μ and use QCD perturbation theory to make predictions at another scale μ'. We will focus on the "track thrust" event shape and compare our calculations to LEP measurements made by the ALEPH [1] and DELPHI [2] Collaborations.

Our previous work in Ref. [10] explained how to interface track functions with fixed-order calculations up to next-to-leading order (NLO). To get reliable predictions for track thrust, we need to include the effects of logarithmic resummation. With the help of soft-collinear effective theory (SCET) [11–14], we obtain results at next-to-leading logarithmic accuracy (NLL) including $\mathcal{O}(\alpha_s)$ fixed-order matching contributions, i.e. up to NLL$'$ order. This turns out to be sufficiently accurate to understand both the qualitative and quantitative behavior of the track thrust distribution.

We will show that ordinary (i.e. calorimeter) thrust and track thrust are remarkably similar, with the leading differences encoded in a small number of nonperturbative parameters. Since an extraction of track functions from data has not yet been performed, we estimate these nonperturbative parameters using Monte Carlo event

generators that have been tuned to LEP data (PYTHIA 8 [15,16] in this study). We find cancellations between the nonperturbative parameters, such that the predicted distributions for calorimeter thrust and track thrust are nearly identical, a feature also seen in LEP data. This behavior could have been anticipated based on the observation in Ref. [10] that hadronization effects are strongly correlated between the numerator and denominator of dimensionless track-based ratios. We can now put this qualitative observation on a firmer quantitative footing.

An interesting theoretical feature of our calculation is that hadronization effects enter directly into the track thrust resummation. In particular, nonperturbative track parameters appear in the anomalous dimensions of the (track-based) jet and soft functions, two important objects in the factorization theorem for the track thrust distribution. As a nice consistency check of our formalism, we find that the hard, jet, and soft anomalous dimensions still cancel, despite the appearance of these parameters. We also show how to incorporate the leading nonperturbative power correction in the track thrust distribution.

This paper is structured as follows. Section II contains a summary of our results and the most significant plots, including a comparison to LEP data. The underlying technical details are discussed in the rest of the paper. We review our track function formalism in Sec. III and calculate track thrust at $\mathcal{O}(\alpha_s)$ in Sec. IV. In Sec. V we present the factorization theorem for track thrust as well as the ingredients needed for a resummation up to NLL′ order in SCET, with details on the RG evolution given in the appendices. A simple expression for track thrust at NLL order is derived in Sec. VI, which allows us to better understand the similarity between calorimeter and track thrust. Our final numerical results are presented in Sec. VII. We conclude in Sec. VIII with a discussion of possible generalizations of our results to other track-based observables.

II. SUMMARY OF RESULTS

To begin, we define the two main event shapes used in our study: calorimeter thrust τ and track thrust $\bar{\tau}$. The classic event shape thrust [17] is defined as

$$T = \max_{\hat{t}} \frac{\sum_i |\hat{t} \cdot \vec{p}_i|}{\sum_i |\vec{p}_i|}, \qquad (1)$$

where the sum runs over all final-state hadrons with momenta $\vec{p}_i$, and the unit vector $\hat{t}$ defines the thrust axis. It is more convenient to work with

$$\tau \equiv 1 - T = \min_{\hat{t}} \frac{\sum_i (|\vec{p}_i| - |\hat{t} \cdot \vec{p}_i|)}{\sum_i |\vec{p}_i|}, \qquad (2)$$

which we will refer to as "thrust" from now on. Since this is measured using all final-state hadrons (charged plus neutral), we call τ "calorimeter thrust." Track thrust $\bar{\tau}$ is defined analogously to Eq. (2), except that the sum over i is
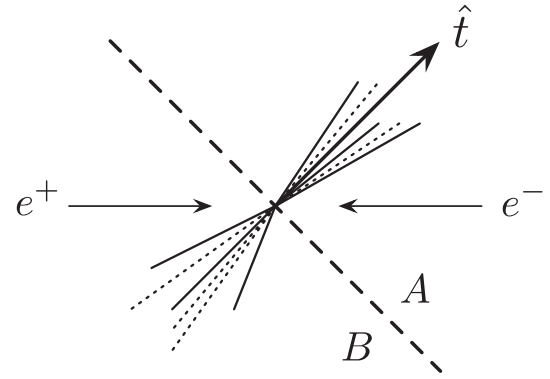

FIG. 1. Illustration of the track thrust measurement in an e^+e^- event with jets initiated by a $q\bar{q}$ pair. Solid lines indicate charged particles and dashed lines indicate neutral particles. For track thrust, the thrust axis $\hat{t}$ is determined by the charged particles alone. The event is divided into hemispheres A and B by a plane perpendicular to the thrust axis.

restricted to charged particles in both the numerator and the denominator. In this paper, a bar will always indicate a track-based quantity.

For the later discussion of the factorization theorem for track thrust in Sec. V, it will be convenient to rewrite thrust in terms of contributions from hemispheres A and B, separated by a plane perpendicular to the thrust axis. The relevant kinematics are illustrated in Fig. 1. Fixing two light-cone vectors n^μ and $\bar{n}^\mu$ such that $n \cdot \bar{n} = 2$, the light-cone components of any four-vector w^μ are given by $w^+ = n \cdot w$, $w^- = \bar{n} \cdot w$, and $w_\perp^\mu$, such that

$$w^\mu = w^+ \frac{\bar{n}^\mu}{2} + w^- \frac{n^\mu}{2} + w_\perp^\mu. \qquad (3)$$

Choosing $n^\mu = (1, 0, 0, 1)$ and $\bar{n}^\mu = (1, 0, 0, -1)$ with the 3-axis aligned along $\hat{t}$, we can rewrite Eq. (2) for tracks as

$$\bar{\tau} = \frac{2(\bar{k}_A^+ + \bar{k}_B^-)}{(x_A + x_B)Q}. \qquad (4)$$

Here, Q is the e^+e^- center-of-mass energy, $x_{A,B}$ are the energy fractions of charged particles in the respective hemispheres, and $\bar{k}_A^+ = \bar{k}_A^0 - \bar{k}_A^3$ and $\bar{k}_B^- = \bar{k}_B^0 + \bar{k}_B^3$ are the small light-cone momentum components of all charged particles in hemisphere A and B, respectively. In this paper, we ignore the subtleties of hadron masses and measurement schemes, which will affect power corrections (see Refs. [18,19]).

At LEP, differential cross sections for calorimeter thrust τ and track thrust $\bar{\tau}$ were measured at both ALEPH [1] and DELPHI [2] on the Z pole ($Q = 91$ GeV). (To our knowledge, these are the only two experiments with public data on track thrust.) In both experiments, measurements were unfolded to the hadron level (including both charged and neutral hadrons for τ, and only charged hadrons for $\bar{\tau}$). The ALEPH and DELPHI normalized distributions are shown in Fig. 2, where we note a remarkable similarity between
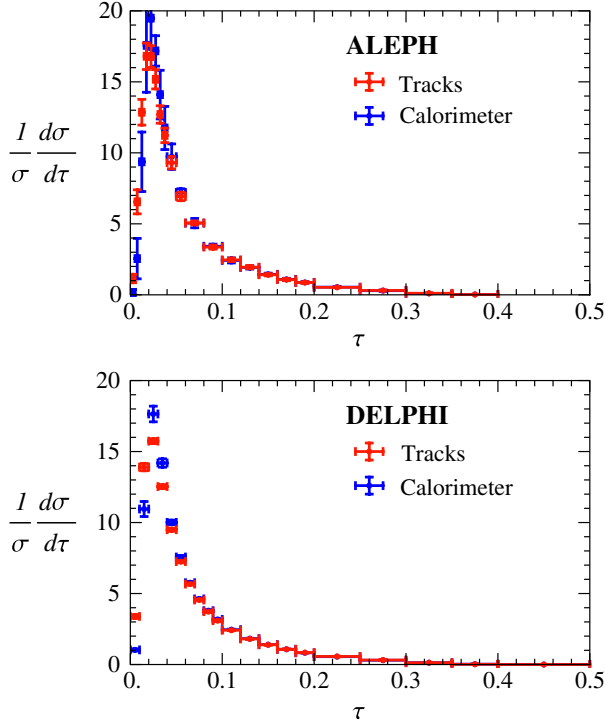
FIG. 2 (color online). ALEPH (top) and DELPHI (bottom) measurements of calorimeter and track thrust. Error bars correspond to the statistical and systematic uncertainties added in quadrature. The experimental uncertainties associated with the track-based measurements are noticeably smaller.

FIG. 3 (color online). Top: NLL′ distributions for calorimeter and track thrust including the leading nonperturbative correction Ω_1^τ. Next-to-leading logarithmic resummation is included together with $\mathcal{O}(\alpha_s)$ fixed-order matching contributions. The NLL′ calculation exhibits the same qualitative similarity between calorimeter and track thrust as seen in LEP data. Bottom: comparing our analytic results to the DELPHI measurement. There is good quantitative agreement in the tail region where our NLL′ calculation is most accurate. The theoretical uncertainties are from scale variation alone, and do not include the (correlated) uncertainties in α_s or Ω_1^τ, nor uncertainties in our track function extraction.

the calorimetric and track-based measurements. Indeed, for all bins outside of the peak region, the distributions are compatible within error bars, and a key goal of this paper is to gain an analytic understanding for why the τ and $\bar{\tau}$ distributions are so similar. Note also that the experimental uncertainty is significantly smaller for the thrust measurements made using tracks.

In Fig. 3, we show the main result of the paper: the resummed NLL′ distributions for calorimeter and track thrust. The latter was obtained using track functions extracted from PYTHIA 8, which itself was tuned to LEP data. The effects of the leading nonperturbative power correction are included through the parameters Ω_1^τ and $\bar{\Omega}_1^\tau$, which are different for calorimeter and track thrust. Interestingly, the NLL′ distributions exhibit the qualitative similarity seen in data between calorimeter thrust and track thrust. We also see excellent quantitative agreement between our result and DELPHI measurements in the peak and tail regions. To the left of the peak there are deviations due to important nonperturbative corrections and in the far-tail region our calculation is missing (known) higher-order perturbative effects.

We now briefly discuss why the τ and $\bar{\tau}$ distributions are so similar, referring the reader to Sec. VI for further details. In Eq. (4), the numerator is dominated by soft gluon emissions which broaden the hemisphere jets, whereas the denominator is mainly affected by fragmentation of
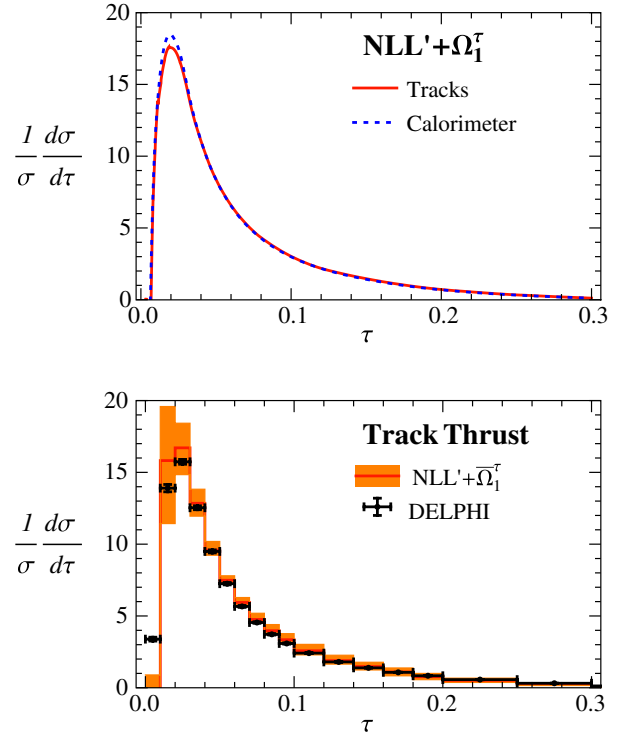
the energetic quark and antiquark emerging from the underlying scattering process. These effects are thus controlled by different track functions (gluon vs. quark) but nearly cancel each other out due to the specific form of the (PYTHIA-based) track functions.

This cancellation is best understood by studying the resummed form of cumulative distributions

$$\Sigma(\tau^c) \equiv \int_0^{\tau^c} d\tau \frac{d\sigma}{d\tau}, \qquad \bar{\Sigma}(\bar{\tau}^c) \equiv \int_0^{\bar{\tau}^c} d\bar{\tau} \frac{d\sigma}{d\bar{\tau}}. \quad (5)$$

As we show in Sec. VI, at NLL the difference between the cumulative distributions (for $\tau^c < 1/3$) is almost entirely captured by

$$\bar{\Sigma}(\bar{\tau}^c) \simeq \Sigma(\tau^c) \times (3\bar{\tau}^c)^\Delta, \quad (6)$$

where the exponent Δ redistributes the cross section between the peak and tail regions. In terms of the strong coupling constant α_s and the quark color-factor $C_F = 4/3$, the explicit form of Δ is

$$\Delta = \frac{2\alpha_s C_F}{\pi}(g_1^L - q^L), \tag{7}$$

which depends on just two nonperturbative parameters: a logarithmic moment of a single gluon track function g_1^L and a logarithmic moment of two quark track functions q^L. The similarity between the τ and $\bar\tau$ distributions can thus be traced to a cancellation between g_1^L and q^L such that $|\Delta| \simeq 0.004$ [see Eq. (62)].

There are additional effects at NLL' from the fixed-order matching which yield further (small) differences between τ and $\bar\tau$ which are compatible with the ALEPH and DELPHI measurements. The nonperturbative power corrections Ω_1^τ and $\bar\Omega_1^\tau$ lead to a respective shift of the τ and $\bar\tau$ distributions by a very similar amount, but increase the difference in the peak region. Overall, though, the similarity between calorimeter and track thrust is well-described by the NLL distribution, and we expect similar cancellations to occur for a variety of (dimensionless) track-based observables.

III. REVIEW OF TRACK FUNCTION FORMALISM

A rigorous QCD description of track-based observables involves track functions $T_i(x, \mu)$ [10] as key ingredients. A parton (quark or gluon) with flavor index i and four-momentum p_i^μ hadronizes into charged particles (tracks) with total four-momentum $\bar p_i^\mu \equiv x p_i^\mu + \mathcal{O}(\Lambda_{\rm QCD})$. The track function is the distribution in the energy fraction x of all tracks (irrespective of their multiplicity or individual properties), and it is normalized as

$$\int_0^1 dx\, T_i(x, \mu) = 1. \tag{8}$$

We will often refer to x as the track fraction.

In the context of factorization theorems, track functions can be used for track-based observables where partons in the underlying process are well separated, i.e. where their typical pairwise invariant masses are larger than $\Lambda_{\rm QCD}$. In this limit, each parton has its own independent track function, with correlations captured by power corrections (to be discussed more in Sec. V C). The track functions then encode process-independent nonperturbative information about the hadronization. Like a FF or a parton distribution function (PDF), $T_i(x, \mu)$ absorbs infrared (IR) divergences in partonic calculations. It has a well-defined dependence on the RG scale μ through an evolution equation which is closely reminiscent of the jet charge distribution [9].

QCD calculations of track-based observables require the determination of matching contributions from partonic cross sections. First recall that the cross section for an IRC-safe observable e measured using partons has the form

$$\frac{d\sigma}{de} = \sum_N \int d\Pi_N \frac{d\sigma_N}{d\Pi_N} \delta[e - \hat e(\{p_i^\mu\})], \tag{9}$$

where we drop possible convolutions with PDFs to keep the notation simple. Here, Π_N denotes the N-body phase space, $d\sigma_N/d\Pi_N$ is the corresponding partonic cross section, and

$\hat e(\{p_i\})$ implements the measurement on the partonic four-momenta p_i^μ. Since e is IRC safe, a cancellation of final state IR divergences between real and virtual diagrams is guaranteed by the KLN theorem [20,21].

For the same observable measured using only tracks, we can write the cross section in the form

$$\frac{d\sigma}{d\bar e} = \sum_N \int d\Pi_N \frac{d\bar\sigma_N}{d\Pi_N} \int \prod_{i=1}^N dx_i T_i(x_i) \delta[\bar e - \hat e(\{x_i p_i^\mu\})]. \tag{10}$$

Here, the partonic cross section $\bar\sigma_N$ should be thought of as a finite matching coefficient where the IR divergences in σ_N have been removed using some scheme. These IR (collinear) divergences are absorbed by the track function $T_i(x_i)$ (which is similarly scheme-dependent). The universality of collinear divergences in QCD [22–24] guarantees the feasibility of this matching to all orders in α_s. In Ref. [10] we explicitly showed the cancellation of IR-divergent terms in the partonic cross section $e^+e^- \to q\bar qg$, which enters the NLO distribution for the energy fraction of charged particles in e^+e^- collisions.

The (bare) track function is defined in QCD in a fashion analogous to the unpolarized FF (cf. [25,26]). Expressed in terms of light-cone components [see Eq. (3)], the quark track function is

$$T_q(x) = \int dy^+ d^2y_\perp e^{ik^- y^+/2} \frac{1}{2N_c} \sum_{C,N} \delta\left(x - \frac{p_C^-}{k^-}\right)$$
$$\times \mathrm{tr}\left[\frac{\not{\bar n}}{2}\langle 0|\psi(y^+, 0, y_\perp)|CN\rangle\langle CN|\bar\psi(0)|0\rangle\right], \tag{11}$$

where ψ is the quark field, C (N) denote charged (neutral) hadrons, and p_C^- is the large momentum component of all charged particles. As for the FF, gauge invariance requires the addition of eikonal Wilson lines. The factor $1/(2N_c)$ in Eq. (11) comes from averaging over the color and spin of the hadronizing quark. The gluon track function is defined analogously. In d space-time dimensions,

$$T_g(x) = -\frac{1}{(d-2)(N_c^2-1)k^-} \int dy^+ d^2y_\perp e^{ik^- y^+/2}$$
$$\times \sum_{C,N} \delta\left(x - \frac{p_C^-}{k^-}\right) \bar n^\mu \bar n^\nu \langle 0|G_{\mu\lambda}^a(y^+, 0, y_\perp)|CN\rangle$$
$$\times \langle CN|G_\nu^{\lambda,a}(0)|0\rangle, \tag{12}$$

where $G_{\mu\nu} = \sum_a G_{\mu\nu}^a T^a$ is the QCD field-strength tensor and an average over colors and the $(d-2)$ polarizations of the gluon is performed.

For the sake of completeness, we also give SCET expressions for the quark and gluon track functions, given in a form which is invariant under nonsingular gauge transformations. In terms of the SCET n-collinear quark $\chi_n(y)$ and gluon $\mathcal{B}_{n\perp}^\mu(y)$ fields, we obtain

$$T_q(x) = 2(2\pi)^3 \frac{1}{2N_c} \sum_{C,N} \delta\left(x - \frac{p_C^-}{k^-}\right)$$

$$\times \text{tr}\left[\frac{\vec{n}}{2} \langle 0|[\delta(k^- - \bar{\mathcal{P}})\delta^2(\mathcal{P}_\perp)\chi_n(0)]|CN\rangle\right.$$

$$\left. \times \langle CN|\bar{\chi}_n(0)|0\rangle\right], \qquad (13)$$

and

$$T_g(x) = -2(2\pi)^3 \frac{k^-}{(d-2)(N_c^2-1)} \sum_{C,N} \delta\left(x - \frac{p_C^-}{k^-}\right)$$

$$\times \langle 0|[\delta(k^- - \bar{\mathcal{P}})\delta^2(\mathcal{P}_\perp)\mathcal{B}_{n\perp}^{\mu,a}(0)]|CN\rangle$$

$$\times \langle CN|\mathcal{B}_{n\perp,\mu}^a(0)|0\rangle, \qquad (14)$$

where the momentum operators $\bar{\mathcal{P}} = \bar{n} \cdot \mathcal{P}$ ($\mathcal{P}_\perp^\mu$) return the sum of the minus (perpendicular) *label* momentum components of all collinear fields on which they act. For the definition of the SCET fields, we refer the reader to e.g. Ref. [27].

Although the track function is a nonperturbative object, some of its properties can be calculated in perturbation theory. In particular, the RG evolution of the track function follows from its ultraviolet (UV) divergences, as we show below. A partonic calculation of the track function is also necessary for extracting the matching coefficient $\bar{\sigma}_N$ in Eq. (10), by using that this equation holds at both the hadronic and partonic level.

At NLO, we can relate the bare track function $T_{i,\text{bare}}^{(1)}(x)$ to the tree-level track functions $T_j^{(0)}(x_1)$ and $T_k^{(0)}(x_2)$ via a collinear splitting $i \to jk$. As indicated in Fig. 4, this splitting is controlled by the timelike Altarelli-Parisi splitting functions $P_{i \to jk}(x)$ [28]. In pure dimensional regularization with $d = 4 - 2\epsilon$,

$$T_{i,\text{bare}}^{(1)}(x) = \frac{1}{2} \sum_{j,k} \int_0^1 dz \left[\frac{\alpha_s(\mu)}{2\pi}\left(\frac{1}{\epsilon_{\text{UV}}} - \frac{1}{\epsilon_{\text{IR}}}\right)P_{i \to jk}(z)\right]$$

$$\times \int dx_1 dx_2 T_j^{(0)}(x_1) T_k^{(0)}(x_2)$$

$$\times \delta[x - zx_1 - (1-z)x_2]. \qquad (15)$$

If $j = k$, the factor $1/2$ is needed for identical particles, whereas if $j \neq k$ this factor gets cancelled by permutations of the two indices. In contrast to the FF or PDF, the NLO track function gets contributions from both branches of the splitting.

Renormalizing the UV divergences in the $\overline{\text{MS}}$-scheme leads to the following evolution equation for the track function,

$$\mu \frac{d}{d\mu} T_i(x, \mu) = \frac{1}{2} \sum_{j,k} \int_0^1 dz dx_1 dx_2 \frac{\alpha_s(\mu)}{\pi} P_{i \to jk}(z) T_j(x_1, \mu)$$

$$\times T_k(x_2, \mu) \delta[x - zx_1 - (1-z)x_2]. \qquad (16)$$

By solving this, $T_i(x, \mu)$ can be extracted at one scale and RG evolved to another scale, and the evolution preserves
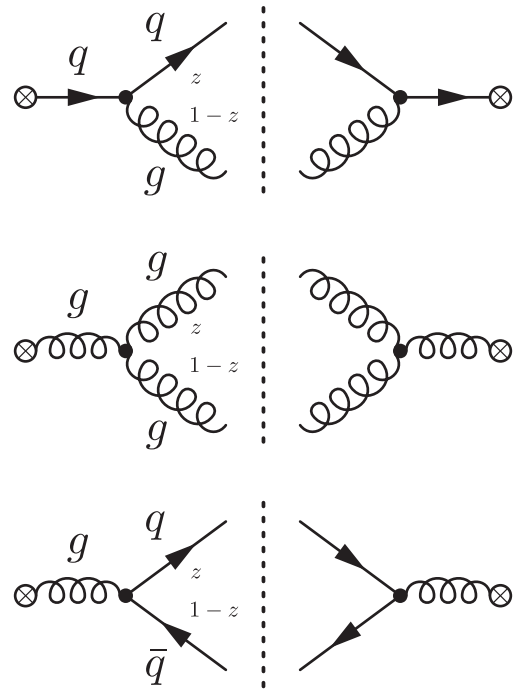

FIG. 4. Perturbative QCD calculation of the quark (top) and gluon (middle and bottom) track functions at NLO from Eqs. (11) and (12) with partonic intermediate states. The NLO track function gets contributions from both branches of the collinear splitting. We do not display virtual diagrams, which vanish in pure dimensional regularization, or diagrams corresponding to Wilson line emissions.

the normalization in Eq. (8). We note that the number of convolutions in the track function RG equation (RGE) grows accordingly to the perturbative order due to multiple branchings, so it becomes numerically more involved to solve this RGE at higher orders. At leading logarithmic (LL) accuracy, the RG evolution in Eq. (16) is equivalent to a parton shower [9], and is in excellent agreement with the parton shower evolution in PYTHIA [10].

Throughout this paper, we determine the track functions used in our analytic formulae using the method of Ref. [10]. That is, we generate pure quark and gluon jet samples with PYTHIA 8.150 [15,16], measure the normalized distribution for the track fraction x within those jets, and extract the track functions by numerically inverting the analytic expression for the same quantity at either LO or NLO. In all of the plots shown here, we use NLO track functions. We emphasize that the use of PYTHIA is not fundamental, and one could imagine extracting the same information from e^+e^- data. That said, since PYTHIA is tuned to LEP data, we expect these track functions to be realistic, but we have not attempted to assign uncertainties to the track functions.

One important point is the choice of α_s. Since we are working at NLL' order in the $\overline{\text{MS}}$ scheme, it would be natural to take the value from Ref. [29] of $\alpha_s(M_Z) = 0.1203 \pm 0.0079$. However, we have extracted the track

functions from PYTHIA 8 whose default value is $\alpha_s(M_Z) = 0.1383$ for the final state parton shower, leading to a formal mismatch between our perturbative and nonperturbative objects. Given the large uncertainties at NLL', we will make an (imperfect) compromise, and extract the NLO track functions from PYTHIA using PYTHIA's value of α_s, but then use

$$\alpha_s(M_Z) = 0.125, \qquad (17)$$

for all subsequent calculations. This choice, along with the leading power correction in Sec. V C, gives a good description of the LEP calorimeter thrust data. As emphasized in Ref. [29], there are strong correlations between the value of α_s and the leading power correction Ω_1^τ, so there are many different choices which would give comparable results; for example the PYTHIA value $\alpha_s(M_Z) = 0.1383$ matches the LEP calorimeter thrust distributions quite well with $\Omega_1^\tau = 0$. A proper treatment of the correlations between these parameters is beyond the scope of this paper, so we will not show the uncertainties associated with $\alpha_s(M_Z)$ or Ω_1^τ.

IV. FIXED-ORDER ANALYSIS OF TRACK THRUST

The leading nontrivial process for thrust at the partonic level is $e^+e^- \rightarrow q\bar{q}g$, which appears at $\mathcal{O}(\alpha_s)$ in a fixed-order expansion. Given an e^+e^- collision at a center-of-mass energy Q, the kinematics of this process are determined by the partonic energy fractions $y_i = 2E_i/Q$ carried by the quark and antiquark, with the gluon energy fraction given by $y_3 = 2 - y_1 - y_2$. From this information, one can readily find the three-momenta of the partons $\vec{p}_1$, $\vec{p}_2$, and $\vec{p}_3$ and determine calorimeter thrust from Eq. (2). For three partons, finding the thrust axis is straightforward, and thrust takes a reasonably simple form

$$\tau = 1 - \frac{\max_{i=1,2,3}|\vec{p}_{CM} - 2\vec{p}_i|}{\sum_i |\vec{p}_i|}, \qquad (18)$$

where we have defined

$$\vec{p}_{CM} \equiv \vec{p}_1 + \vec{p}_2 + \vec{p}_3. \qquad (19)$$

To obtain the charged track three-momenta, one simply rescales the parton momenta by the track fraction x_i,

$$\vec{\tilde{p}}_i = x_i \vec{p}_i. \qquad (20)$$

Track thrust can then be calculated from Eq. (18) with all $\vec{p}$ replaced by $\vec{\tilde{p}}$. Note that in the e^+e^- rest frame, $|\vec{p}_{CM}| = 0$, but $|\vec{\tilde{p}}_{CM}|$ is typically nonzero.

The calculation of the track thrust distribution at $\mathcal{O}(\alpha_s)$ is very similar to the one performed in Ref. [10] for the total charged particle energy fraction. Weighting each parton by the corresponding track function, we find

$$\frac{d\sigma}{d\bar{\tau}} = \int_0^1 dy_1 dy_2 \frac{d\bar{\sigma}(\mu)}{dy_1 dy_2} \int_0^1 dx_1 dx_2 dx_3 T_q(x_1, \mu) T_q(x_2, \mu)$$
$$\times T_g(x_3, \mu) \delta[\bar{\tau} - \bar{\tau}(y_1, y_2, x_1, x_2, x_3)]. \qquad (21)$$

where the measurement function $\bar{\tau}(y_1, y_2, x_1, x_2, x_3)$ implements Eq. (18). Note that $T_q = T_{\bar{q}}$, by charge conjugation. The relevant doubly differential partonic cross section is given in Ref. [10] in the $\overline{MS}$ scheme. Ignoring the singularities at $y_1 = 1$ and $y_2 = 1$ (which only contribute to a delta function at $\bar{\tau} = 0$),

$$\frac{d\bar{\sigma}(\mu)}{dy_1 dy_2} = \sigma_0 \frac{\alpha_s(\mu)C_F}{2\pi} \frac{\theta(y_1 + y_2 - 1)(y_1^2 + y_2^2)}{(1 - y_1)(1 - y_2)} + \cdots. \qquad (22)$$

Here, σ_0 is the total Born cross section

$$\sigma_0 = \frac{4\pi\alpha^2 N_c}{3Q^2}$$
$$\times \left(Q_q^2 + \frac{(v_q^2 + a_q^2)(v_\ell^2 + a_\ell^2) - 2Q_q v_q v_\ell(1 - M_Z^2/Q^2)}{(1 - M_Z^2/Q^2)^2 + M_Z^2\Gamma_Z^2/Q^4}\right), \qquad (23)$$

which depends on the (anti)quark flavor through its electric charge Q_q and vector and axial couplings v_q and a_q to the intermediate vector boson.

In Fig. 5 we compare the calorimeter versus track thrust distributions at $\mathcal{O}(\alpha_s)$, and find that they are remarkably similar. One might wonder if this small difference is a fundamental feature of Eq. (21) or simply an accident of the specific forms of our (PYTHIA-based) track functions. We can test this by calculating track thrust using the following "dummy" track functions,

$$T_q(x, \mu = M_Z) = 30x^4(1 - x),$$
$$T_g(x, \mu = M_Z) = 252x^2(1 - x)^6. \qquad (24)$$

Indeed, the difference in Fig. 6 between track and calorimeter thrust is now large. Thus, the similarity between the τ and $\bar{\tau}$ distributions has to do with the specific properties of the track function. We will be able to achieve a better analytic understanding of why the effect of switching from calorimeter to tracks is so small in Sec. VI.
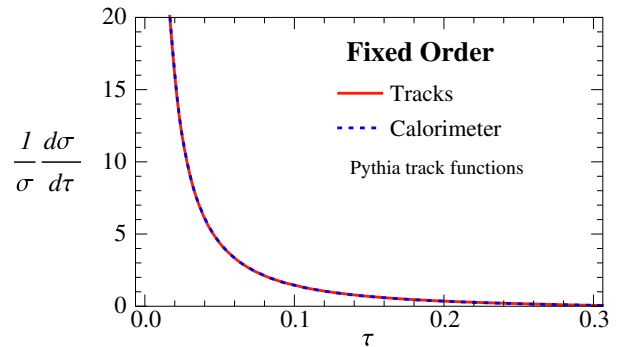

FIG. 5 (color online). Distributions for calorimeter and track thrust from Eq. (21) at $\mathcal{O}(\alpha_s)$. The NLO track functions are extracted from PYTHIA 8.150 [15,16] using the procedure in Ref. [10].
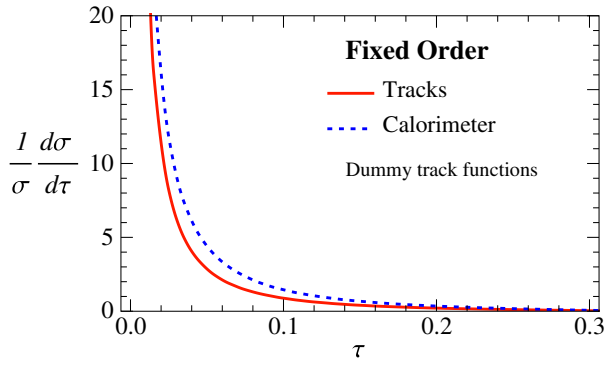
FIG. 6 (color online). Distributions for calorimeter and track thrust using dummy track functions. Comparing to Fig. 5, we conclude that the similarity between τ and $\bar{\tau}$ is due to the specific form of the track function.

V. FACTORIZATION AND RESUMMATION OF TRACK THRUST

The thrust distribution can be divided into three regions: the peak region ($\tau \simeq 2\Lambda_{\rm QCD}/Q$), the tail region ($2\Lambda_{\rm QCD}/Q \ll \tau < 1/3$), and the far-tail region ($1/3 \lesssim \tau \leq 1/2$). For $\tau \simeq 0$, events are described by two narrow back-to-back jets, each carrying about half of the center-of-mass energy. For τ close to the kinematic endpoint $1/2$, the event is characterized by an isotropic multi-particle final state. At $\mathcal{O}(\alpha_s)$ from Sec. IV, the kinematic endpoint is $1/3$ corresponding to three maximally separated jets. We therefore do not obtain a reliable description of the far-tail region.

In this paper, we are interested in properly describing the tail region of the thrust distribution, which dominantly consists of broader dijets and 3-jet events. In this region, the dynamics is governed by three well-separated scales: the *hard scale* ($\mu_H \simeq Q$) which is set by the e^+e^- center-of-mass energy Q, the *jet scale* ($\mu_J \simeq Q\sqrt{\tau}$) which is set by the momentum of the particles transverse to thrust axis, and the *soft scale* ($\mu_S \simeq Q\tau$) which is set by the typical energy of soft radiation between the hard jets. When $\tau \ll 1$, there will be large hierarchies between these scales, so we will need to resum double logarithms of the form $\alpha_s^n \ln^m \tau$ ($m \leq 2n$). Because we focus on the region where $\mu_S \simeq \tau Q \gg \Lambda_{\rm QCD}$, the contribution from soft radiation is accurately described by perturbation theory, with nonperturbative effects captured by a series of power correction parameters. We will only use the leading power correction $\bar{\Omega}_1^\tau$ in our analysis, though if were interested in describing the peak region correctly we would have to include a full nonperturbative shape function, see Sec. V C.

The leading-power factorization theorem for calorimeter thrust is well known [30–33]:

$$\frac{{\rm d}\sigma}{{\rm d}\tau} = \sigma_0 H(Q^2, \mu) \int_0^\infty {\rm d}k\,{\rm d}s_A\,{\rm d}s_B\, S(k, \mu) J(s_A, \mu) J(s_B, \mu)$$

$$\times \delta\left[\tau - \frac{1}{Q}\left(\frac{s_A}{Q} + \frac{s_B}{Q} + k\right)\right]. \tag{25}$$

Here, σ_0 is the Born cross section from Eq. (23), H, J, and S are respectively the hard, jet, and soft functions, $s_{A,B}$ are the invariant mass-squareds of collinear radiation in hemispheres A and B, and k is the contribution to thrust from soft radiation.

The goal of this section is to translate Eq. (25) into a factorization theorem for track thrust. This procedure is made straightforward by applying the matching procedure defined in Eq. (10) to the objects S and J. The final answer is:

$$\frac{{\rm d}\sigma}{{\rm d}\bar{\tau}} = \sigma_0 H(Q^2, \mu) \int_0^\infty {\rm d}\bar{k}\,{\rm d}\bar{s}_A\,{\rm d}\bar{s}_B \int_0^1 {\rm d}x_A\,{\rm d}x_B$$

$$\times \bar{S}(\bar{k}, \mu) \bar{J}(\bar{s}_A, x_A, \mu) \bar{J}(\bar{s}_B, x_B, \mu)$$

$$\times \delta\left[\bar{\tau} - \frac{2}{(x_A + x_B)Q}\left(\frac{\bar{s}_A}{Q} + \frac{\bar{s}_B}{Q} + \bar{k}\right)\right]. \tag{26}$$

We now explain each of the ingredients in this formula, with details to appear in the subsequent subsections.

The delta function in Eq. (26) comes from the form of $\bar{\tau}$ given in Eq. (4). Dividing phase space into hemispheres A and B defined by the thrust axis, track thrust depends on the track fractions x_i, the rescaled track invariant mass-squared of collinear radiation $\bar{s}_i = s_i^{\rm tracks}/x_i$, and the track soft contribution $\bar{k}$. The reason we are using the rescaled $\bar{s}_i$ (and not $s_i^{\rm tracks}$ directly) is that $\bar{s}_A = Q\bar{k}_A^+$ and $\bar{s}_B = Q\bar{k}_B^-$ directly enter the definition of track thrust.

The hard function $H(Q^2, \mu)$ is the same as for calorimeter thrust and encodes virtual effects arising from the production of the $q\bar{q}$ pair at the hard scale. We give the form of H in Sec. V A.

The track thrust soft function $\bar{S}(\bar{k}, \mu)$, where $\bar{k} = \bar{k}_A^+ + \bar{k}_B^-$, describes the contribution to track thrust due to soft parton emissions which then hadronize into tracks. At NLO, soft radiation consists of only a single gluon emission so we can simply rescale

$$\bar{k} = xk, \tag{27}$$

where x is the track fraction of the gluon. This leads to a straightforward relationship between the ordinary thrust soft function and the track-based version, as discussed in Sec. V B. At higher orders, the expression for $\bar{k}$ will become more complicated. The track-based soft function also incorporates information about nonperturbative physics through power corrections, and we discuss the leading power correction $\bar{\Omega}_1^\tau$ in Sec. V C.

The track-based jet function $\bar{J}(\bar{s}, x, \mu)$ encodes the (real and virtual) collinear radiation in each hemisphere. At NLO, a hemisphere jet consist of just two partons, so

$$\bar{s}_i = \frac{x_1 x_2}{x_i} s_i, \tag{28}$$

where x_1 and x_2 are the track fractions of the two partons, x_i is the track fraction of the hemisphere ($i = A, B$), and s_i is the (calorimeter) invariant mass of the hemisphere.

Unlike the calorimetric version, $\bar{J}$ depends not only on the rescaled track invariant mass $\bar{s}$ (given by Eq. (28) at NLO), but also on the track fraction x. For this reason, the track-based jet function is considerably more complicated than the usual jet function, and requires a more complicated matching calculation, as described in Sec. V D.

In order to resum logarithms, we not only need the forms of the H, $\bar{J}$, and $\bar{S}$, but also their anomalous dimensions. At LL order, this means incorporating the one-loop cusp anomalous dimension to resum the Sudakov double logs. In this paper, we incorporate NLL resummation, which includes the two-loop cusp and the one-loop noncusp anomalous dimension terms. Correspondingly, the running of α_s is consistently implemented at two loops, using the Z pole value for α_s in Eq. (17). Track thrust resummation is very similar to the calorimetric case, as discussed in Sec. VI and the appendices. The main difference is that the anomalous dimensions of $\bar{J}$ and $\bar{S}$ now depend on nonperturbative parameters.

In addition to the ingredients above, we will incorporate fixed-order nonsingular corrections described in Sec. V F. Following the primed counting scheme of Ref. [29], fixed-order matching contributions are included at one order higher in the expansion in α_s compared to the usual (non-primed) counting. Here we work to NLL' order which incorporates all of the $\mathcal{O}(\alpha_s)$ terms contained in Eq. (21).

A. Hard function

At leading order in the electroweak interactions, the hard function is given by the square of the Wilson coefficient in the matching of the quark current from QCD onto SCET [34,35],

$$H(Q^2, \mu) = 1 + \frac{\alpha_s(\mu)C_F}{2\pi}$$
$$\times \left[-\ln^2\left(\frac{Q^2}{\mu^2}\right) + 3\ln\left(\frac{Q^2}{\mu^2}\right) - 8 + \frac{7\pi^2}{6} \right]. \quad (29)$$

The anomalous dimension of this object is

$$\mu\frac{d}{d\mu}H(Q^2, \mu) = \gamma_H(Q^2, \mu)H(Q^2, \mu),$$

$$\gamma_H(Q^2, \mu) = 2\Gamma_{\text{cusp}}[\alpha_s(\mu)]\ln\frac{Q^2}{\mu^2} + \gamma_H[\alpha_s(\mu)],$$

$$\gamma_H[\alpha_s] = -\frac{3\alpha_s C_F}{\pi}. \quad (30)$$

The cusp anomalous dimension Γ_{cusp} is given in Eqs. (A6) and (A7). We will use the noncusp γ_H to perform a consistency check on our factorization theorem in Eq. (51).

B. Soft function

At NLO, there is only one soft gluon emission, so in order to obtain the soft function, we can simply convolve the NLO thrust soft function with the gluon track function,

$$\bar{S}(\bar{k}, \mu) = \int_0^\infty dk\, S(k, \mu) \int_0^1 dx\, T_g(x, \mu)\delta(\bar{k} - xk), \quad (31)$$

where we have used the relationship between the kinematics in Eq. (27). This is the simplest possible version of the matching equation in Eq. (10).

The ordinary thrust soft function S is defined through the vacuum matrix element of eikonal Wilson lines and its one-loop perturbative expression for calorimeter thrust can be obtained from Refs. [33,36],

$$S(k, \mu) = \delta(k) + \frac{\alpha_s(\mu)C_F}{2\pi}\left[-\frac{8}{\mu}\mathcal{L}_1\left(\frac{k}{\mu}\right) + \frac{\pi^2}{6}\delta(k) \right], \quad (32)$$

where the plus distributions $\mathcal{L}_n$ are defined in Appendix C.

Using Eq. (31), the corresponding track-based version $\bar{S}$ is given by

$$\bar{S}(\bar{k}, \mu) = \int_0^1 \frac{dx}{x} T_g(x, \mu)\Bigg(\delta(\bar{k}/x)$$
$$+ \frac{\alpha_s C_F}{2\pi}\left[-\frac{8}{\mu}\mathcal{L}_1\left(\frac{\bar{k}}{x\mu}\right) + \frac{\pi^2}{6}\delta(\bar{k}/x) \right]\Bigg)$$
$$= \delta(\bar{k}) + \frac{\alpha_s C_F}{2\pi}\left[-\frac{8}{\mu}\mathcal{L}_1\left(\frac{\bar{k}}{\mu}\right) + \frac{8g_1^L}{\mu}\mathcal{L}_0\left(\frac{\bar{k}}{\mu}\right) \right.$$
$$\left. + \left(\frac{\pi^2}{6} - 4g_2^L\right)\delta(\bar{k}) \right]. \quad (33)$$

While one naively might think that $\bar{S}$ would depend on the entire track function, from the rescaling properties of the plus distributions in Eq. (C4), we see that only two logarithmic moments of the gluon track function appear in the soft function, namely g_1^L and g_2^L, defined as

$$g_n^L(\mu) \equiv \int_0^1 dx\, T_g(x, \mu)\ln^n x. \quad (34)$$

From Eq. (33), we can derive the anomalous dimension of the track soft function

$$\mu\frac{d}{d\mu}\bar{S}(\bar{k}, \mu) = \int_0^{\bar{k}} d\bar{k}'\, \gamma_{\bar{S}}(\bar{k} - \bar{k}', \mu)\bar{S}(\bar{k}', \mu),$$

$$\gamma_{\bar{S}}(\bar{k}, \mu) = 4\Gamma_{\text{cusp}}[\alpha_s(\mu)]\frac{1}{\mu}\mathcal{L}_0\left(\frac{\bar{k}}{\mu}\right) + \gamma_{\bar{S}}[\alpha_s(\mu)]\delta(k),$$

$$\gamma_{\bar{S}}[\alpha_s] = -\frac{4\alpha_s C_F}{\pi}g_1^L. \quad (35)$$

Interestingly, the noncusp anomalous dimension depends on the logarithmic moment g_1^L of the gluon track function. This arises because the RG evolution sums multiple emissions, and thus the effect of the hadronization of these emissions must be exponentiated. Note that g_1^L depends (weakly) on the renormalization scale μ, but this effect is beyond the order that we are working.

C. Leading power correction

In the tail region of the thrust distribution, nonperturbative physics is captured via power corrections. As we will now review, the leading power correction simply acts as a

shift of the soft function in Eq. (33) by an amount proportional to Λ_{QCD} [37–40]. The amount of the shift is different for calorimeter and track thrust, but the essential formalism is the same in both cases.

Given a hadronic final state with charged hadrons C and neutral hadrons N, we define a calorimeter measurement operator

$$\hat{k}|CN\rangle = \sum_{i \in C,N} (|\vec{p}_i| - |\hat{t} \cdot \vec{p}_i|)|CN\rangle, \qquad (36)$$

where the sum runs over all hadrons in C and N, $\hat{t}$ is the thrust axis, and $\vec{p}_i$ is the three-momentum for hadron i. This operator measures the numerator of Eq. (2). The track measurement operator is almost the same, but the sum only runs over the charged hadrons C.

The soft function S describes the cross section to produce a measurement k in the presence of back-to-back eikonal quarks. Formally, it is defined as

$$S(k, \mu) = \frac{1}{N_c} \langle 0|\text{tr}\bar{Y}_{\bar{n}}^T Y_n \delta(k - \hat{k}) Y_n^\dagger \bar{Y}_{\bar{n}}^*|0\rangle, \qquad (37)$$

where $Y_n^\dagger(0) = \text{P}\exp(ig \int_0^\infty ds\, n \cdot A(ns))$ is a (ultra)soft Wilson line in the fundamental representation, $\bar{Y}_{\bar{n}}^\dagger$ is the analogue in the $\bar{3}$ representation, and the trace is taken over color indices.

For an additive observable like thrust, the soft function factorizes into a partonic perturbative part S^{part} [calculated already in Eq. (32)] and a nonperturbative part S^{NP} (also called the shape function [31,41–43])

$$S(k) = \int_0^\infty d\ell\, S^{\text{part}}(k - \ell) S^{\text{NP}}(\ell). \qquad (38)$$

In the tail region where $k \simeq Q\tau \gg \Lambda_{\text{QCD}}$, we can perform an operator product expansion (OPE) on $S^{\text{NP}}(\ell)$

$$S^{\text{NP}}(\ell) = \delta(\ell) - \delta'(\ell)\Omega_1^\tau + \cdots, \qquad (39)$$

where the leading power correction for thrust $\Omega_1^\tau \simeq \Lambda_{\text{QCD}}$ is defined via the nonperturbative matrix element

$$\Omega_1^\tau = \frac{1}{N_c} \langle 0|\text{tr}\bar{Y}_{\bar{n}}^T(0) Y_n(0) \hat{k} Y_n^\dagger(0) \bar{Y}_{\bar{n}}^*(0)|0\rangle. \qquad (40)$$

The full soft function in Eq. (38) can then be approximated as a shift

$$S(k) \simeq S^{\text{part}}(k - \Omega_1^\tau) + \mathcal{O}\left(\frac{\alpha_s \Lambda_{\text{QCD}}}{k^2}\right) + \mathcal{O}\left(\frac{\Lambda_{\text{QCD}}^2}{k^3}\right). \qquad (41)$$

This in turn leads to an overall shift in the thrust distribution, whose effect is most prominent at small τ.

The formalism above applies equally well to calorimeter thrust and track thrust. Focussing on calorimeter thrust, the value of Ω_1^τ must be extracted from data, since it is a fundamentally nonperturbative parameter. Typically, one expresses Ω_1^τ in terms of the universal power correction Ω_1 [40,44,45]

$$\Omega_1^\tau \equiv 2\Omega_1, \qquad (42)$$

though strictly speaking, Ω_1 is only universal for measurements in the same universality class (see Ref. [19]). Putting aside that subtlety, the analysis in Ref. [29] extracted a value of $\Omega_1 = 0.264 \pm 0.213$ GeV in the $\overline{\text{MS}}$ scheme at NLL$'$ from fits to (calorimeter) thrust data. We will therefore take a value of

$$\Omega_1^\tau = 0.5 \text{ GeV} \qquad (43)$$

for our analysis of calorimeter thrust. As mentioned near Eq. (17), there are strong correlations between α_s and Ω_1^τ, and this choice gives a reasonable (but not perfect) description of LEP data.

For track thrust, we estimate that the parameter $\bar{\Omega}_1^\tau$ entering the analogous OPE for $\bar{S}^{\text{NP}}(\bar{k})$ is given by

$$\bar{\Omega}_1^\tau \simeq \langle x\rangle \Omega_1^\tau = 0.3 \text{ GeV}, \qquad (44)$$

where we have taken the average track fraction $\langle x\rangle$ to be 0.6 [10]. This approximation is only justified if the matrix element defining $\bar{\Omega}_1^\tau$ is dominated by a single gluon emission and if the gluon track function has a narrow width. More generally, $\bar{\Omega}_1^\tau$ will encode hadronization correlations.

We emphasize that we have applied this nonperturbative shift $\bar{\Omega}_1^\tau$ to the track-based soft function directly,

$$\bar{S}(\bar{k}, \mu) \simeq \bar{S}^{\text{part}}(\bar{k} - \bar{\Omega}_1^\tau, \mu). \qquad (45)$$

Note that a shift in the track soft function $\bar{S}(\bar{k})$ does not amount to an overall shift of the whole track thrust distribution due to the more complicated convolution structure in Eq. (26). Looking at Eq. (31), we could have tried to apply the usual shift Ω_1^τ to S instead, but this would have ignored the important fact that the track function T_g itself has nonperturbative power corrections. The power correction $\bar{\Omega}_1^\tau$ includes both of these effects. For the subleading power corrections (beyond the scope of this paper), it may or may not be preferable to separately treat the nonperturbative corrections to S and T_g.

D. Jet function

For the collinear radiation, described by the jet function, we need both the dependence on the energy fraction x of the collinear tracks as well as their contribution to the rescaled hemisphere track invariant mass-squared $\bar{s}$. The NLO jet function consists of one perturbative $q \to qg$ splitting whose branches hadronize independently. To carry out the matching in Eq. (10), we can use the matching coefficient $\mathcal{J}_{qq}(s, z, \mu)$ given in Refs. [27,46], since the cancellation of IR divergences proceeds in an identical manner. Here, s is the qg invariant mass and z is the momentum fraction of the final quark. Inserting this matching coefficient into Eq. (10), the matching calculation yields

$$\bar{J}(\bar{s}, x, \mu) = \int_0^\infty \mathrm{d}s \int_0^1 \mathrm{d}z \frac{\mathcal{J}_{qq}(s, z, \mu)}{2(2\pi)^3}$$

$$\times \int_0^1 \mathrm{d}x_1 \mathrm{d}x_2 T_q(x_1, \mu) T_g(x_2, \mu)$$

$$\times \delta[x - zx_1 - (1-z)x_2]\delta\left(\bar{s} - \frac{x_1 x_2}{x} s\right), \qquad (46)$$

where we have used the kinematics in Eq. (28). The same coefficients $\mathcal{J}_{ij}(s, z, \mu)$ also appeared in the description of the fragmentation of a hadron inside a jet [27,47], as they describe the perturbative splittings building up the jet radiation.

The expression for the matching coefficient is [27,46]

$$\frac{\mathcal{J}_{qq}(s, z, \mu)}{2(2\pi)^3} = \delta(s)\delta(1-z) + \frac{\alpha_s(\mu)C_F}{2\pi}\left\{\frac{2}{\mu^2}\mathcal{L}_1\left(\frac{s}{\mu^2}\right)\delta(1-z) + \frac{1}{\mu^2}\mathcal{L}_0\left(\frac{s}{\mu^2}\right)(1+z^2)\mathcal{L}_0(1-z)\right.$$

$$\left. + \delta(s)\left[(1+z^2)\mathcal{L}_1(1-z) + \frac{1+z^2}{1-z}\ln z + 1 - z - \frac{\pi^2}{6}\delta(1-z)\right]\right\}, \qquad (47)$$

so evaluating Eq. (46), we obtain

$$\bar{J}(\bar{s}, x, \mu) = \left(\delta(\bar{s}) + \frac{\alpha_s C_F}{2\pi}\left[\frac{2}{\mu^2}\mathcal{L}_1\left(\frac{\bar{s}}{\mu^2}\right) - \frac{2g_1^L}{\mu^2}\mathcal{L}_0\left(\frac{\bar{s}}{\mu^2}\right) + \delta(\bar{s})\left(g_2^L - \frac{\pi^2}{6}\right)\right]\right)T_q(x)$$

$$+ \frac{\alpha_s C_F}{2\pi}\int_0^1 \mathrm{d}x_2 \int_0^1 \frac{\mathrm{d}z}{z}\left\{\frac{1}{\mu^2}\mathcal{L}_0\left(\frac{\bar{s}}{\mu^2}\right)(1+z^2)\mathcal{L}_0(1-z) + \delta(\bar{s})\left[(1+z^2)\mathcal{L}_1(1-z)\right.\right.$$

$$\left.\left. + \ln\left(\frac{xz^2}{[x-(1-z)x_2]x_2}\right)(1+z^2)\mathcal{L}_0(1-z) + 1 - z\right]\right\}T_q\left(\frac{x-(1-z)x_2}{z}\right)T_g(x_2). \qquad (48)$$

Here we use that the track function vanishes outside the range $x \in [0, 1]$ to avoid writing explicit Heaviside functions. Unlike the soft function, the jet function depends on the full functional form of the quark and gluon track functions, and not just the logarithmic moments. To perform these integrals numerically, we used the CUBA package [48].

The corresponding anomalous dimension is given by

$$\mu\frac{\mathrm{d}}{\mathrm{d}\mu}\bar{J}(\bar{s}, x, \mu) = \int_0^{\bar{s}}\mathrm{d}\bar{s}'\gamma_{\bar{J}}(\bar{s} - \bar{s}', \mu)\bar{J}(\bar{s}', x, \mu),$$

$$\gamma_{\bar{J}}(\bar{s}, \mu) = -2\Gamma_{\mathrm{cusp}}[\alpha_s(\mu)]\frac{1}{\mu^2}\mathcal{L}_0\left(\frac{\bar{s}}{\mu^2}\right)$$

$$+ \gamma_{\bar{J}}[\alpha_s(\mu)]\delta(\bar{s}),$$

$$\gamma_{\bar{J}}[\alpha_s] = \frac{\alpha_s C_F}{\pi}\left(2g_1^L + \frac{3}{2}\right). \qquad (49)$$

Note that the evolution only affects $\bar{s}$ and not x. As for the soft function, the logarithmic moment of the gluon track function g_1^L contributes to the noncusp anomalous dimension.

E. Resummation

In the effective field theory approach we follow here, the resummation of large double logarithms $\alpha_s^n \ln^m \tau$ $(m \leq 2n)$ is achieved by evaluating the hard, jet, and soft functions at their natural scales μ_H, μ_J, and μ_S where they contain no large logarithms, and running them to a common scale μ using their respective RG equations.

These RG evolution kernels were implicit in the cross section in Eq. (26) and are given in Appendix A. Explicitly including them,

$$\frac{\mathrm{d}\sigma}{\mathrm{d}\bar{\tau}} = \sigma_0 H(Q^2, \mu_H)U_H(Q^2, \mu_H, \mu)$$

$$\times \int \mathrm{d}\bar{s}_A \mathrm{d}\bar{s}'_A \bar{J}(\bar{s}_A - \bar{s}'_A, \mu_J)U_{\bar{J}}(\bar{s}'_A, \mu_J, \mu)$$

$$\times \int \mathrm{d}\bar{s}_B \mathrm{d}\bar{s}'_B \bar{J}(\bar{s}_B - \bar{s}'_B, \mu_J)U_{\bar{J}}(\bar{s}'_B, \mu_J, \mu)$$

$$\times \int \mathrm{d}\bar{k}\mathrm{d}\bar{k}' \bar{S}(\bar{k} - \bar{k}', \mu_S)U_{\bar{S}}(\bar{k}', \mu_S, \mu)$$

$$\times \delta\left[\bar{\tau} - \frac{2}{(x_A + x_B)Q}\left(\frac{\bar{s}_A}{Q} + \frac{\bar{s}_B}{Q} + \bar{k}\right)\right]. \qquad (50)$$

Consistency of the factorization theorem requires that the cross section is μ-independent at the order that we are working, implying a cancellation between the anomalous dimensions. For the cusp anomalous dimension, this cancellation is the same as for calorimeter thrust. For the noncusp pieces from Eqs. (30), (35), and (49), there are additional terms involving g_1^L in $\gamma_{\bar{S}}$ and $\gamma_{\bar{J}}$, but they cancel in the sum

$$\gamma_H^{\mathrm{noncusp}} + 2\gamma_{\bar{J}}^{\mathrm{noncusp}} + \gamma_{\bar{S}}^{\mathrm{noncusp}} = 0, \qquad (51)$$

to fulfill consistency requirements.

An important question is the choice of scales μ_H, μ_J, and μ_S to use in this formula. While our focus is on the tail region of the thrust distribution, where $\mu_H \simeq Q$, $\mu_J \simeq \sqrt{\tau}Q$ and $\mu_S \simeq \tau Q$, we do want our formulas to be

accurate for all values of τ. Since there are three distinct kinematic regions characterizing the thrust distribution, the resummation of the logarithms of τ must be handled in different ways. A smooth transition between the three regions is achieved through profile functions [29,43] as described in Appendix B. Our choice of the profile parameters is such that resummation is turned off at $\bar{\tau} \simeq 1/3$, which is the $\mathcal{O}(\alpha_s)$ endpoint from Sec. IV. (This is in contrast to the higher-order calculation in Refs. [29,49] where the resummation is only turned off at the true endpoint $\tau \simeq 1/2$.)

For the plots in Sec. VII, we calculate the cumulative version of Eq. (50)

$$\bar{\Sigma}(\bar{\tau}^c) \equiv \int_0^{\bar{\tau}^c} d\bar{\tau} \frac{d\sigma}{d\bar{\tau}} \qquad (52)$$

at NLL′ using the scales μ_H, μ_J, and μ_S set by the value of $\bar{\tau}^c$. We then take the numerical derivative of $\bar{\Sigma}(\bar{\tau}^c)$ to find the track thrust distribution (see Ref. [29] for a discussion of alternative choices). This derivative picks up both the explicit $\bar{\tau}$-dependence as well as the implicit $\bar{\tau}$-dependence of our scale choice for μ_H, μ_J, and μ_S. The differential version in Eq. (50) misses the latter contribution, though it is a small effect.

F. Nonsingular contribution

The factorization theorem in Eqs. (26) and (50) includes all the terms in the track thrust distribution that are singular in τ as $\tau \to 0$. There is an additional nonsingular contribution of $\mathcal{O}(\tau)$, which is thus important in the endpoint region. This contribution needs to be included to have our distribution formally accurate to $\mathcal{O}(\alpha_s)$ and is the last step in attaining NLL′ accuracy.

We can extract the nonsingular corrections by subtracting the singular terms [obtained from setting $\mu_H = \mu_J = \mu_S = \mu$ in Eq. (26)] from the fixed-order $\mathcal{O}(\alpha_s)$ cross section in Eq. (21). At the level of the cumulative cross section in Eq. (52),

$$\bar{\Sigma}_{ns}(\bar{\tau}^c) = \bar{\Sigma}_{FO}(\bar{\tau}^c) - \bar{\Sigma}_{sing}(\bar{\tau}^c). \qquad (53)$$
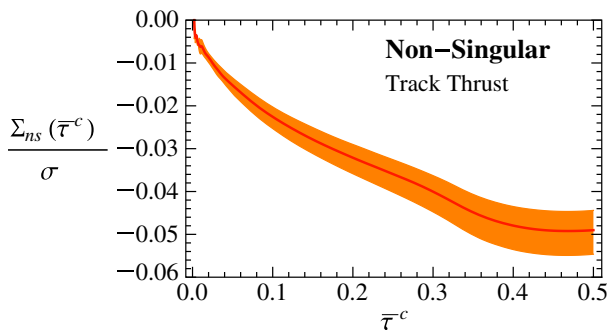

FIG. 7 (color online). Nonsingular contribution to the normalized cumulative thrust distribution at $\mathcal{O}(\alpha_s)$. The central value corresponds to $\mu = M_Z$, with the uncertainty bands from varying $\mu \in [M_Z/2, 2M_Z]$.

Our extraction of $\bar{\Sigma}_{ns}(\bar{\tau}^c)$ is shown in Fig. 7. The fact that $\bar{\Sigma}_{ns}(\bar{\tau}^c = 0) = 0$ provides another consistency check of our formalism, showing that our factorization formula successfully reproduces the singular part of the $\mathcal{O}(\alpha_s)$ cross section. We use $\mu = M_Z$ as the central value for extracting $\bar{\Sigma}_{ns}(\bar{\tau}^c)$, and estimate perturbative uncertainties by varying μ between $M_Z/2$ and $2M_Z$.

VI. SIMPLIFICATIONS AT NLL

In both the LEP data in Fig. 2 and the fixed-order calculation in Fig. 5, we saw a remarkable similarity between the calorimeter and track thrust distributions. We will now try to understand this from our resummed calculation by looking at the leading effect of switching to tracks.

The first nontrivial order in the resummed distribution is NLL. This consists of evaluating Eq. (50) with only the leading order hard, jet, and soft functions, but including the subleading evolution kernels. Using the solutions to the RG equations in Appendix A, the NLL cumulative distribution is

$$\bar{\Sigma}(\bar{\tau}^c) = \sigma_0 e^{K_H} \left(\frac{Q^2}{\mu_H^2}\right)^{\eta_H} \frac{e^{K_{\bar{S}} - \gamma_E \eta_{\bar{S}}}}{\Gamma(1 + \eta_{\bar{S}})} \left(\frac{Q\bar{\tau}^c}{\mu_S}\right)^{\eta_{\bar{S}}}$$
$$\times \int dx_A dx_B T_q(x_A, \mu_J) T_q(x_B, \mu_J) \left(\frac{x_A + x_B}{2}\right)^{\eta_{\bar{S}}}, \qquad (54)$$

where γ_E is Euler's constant, and we have chosen to evolve the hard and soft scales to the jet scale μ_J. The functions $K_H(\mu_H, \mu_J)$, $\eta_H(\mu_H, \mu_J)$, $K_{\bar{S}}(\mu_S, \mu_J)$ and $\eta_{\bar{S}}(\mu_S, \mu_J)$ are given in Appendix A and depend on our choice for μ_H, μ_J, and μ_S, which we discuss below. Note that this expression contains an explicit dependence on the quark track functions T_q since they appear in the tree-level jet functions. Eq. (54) contains only the information needed at NLL accuracy, and therefore does not include the leading hadronization power correction or nonsingular contributions.

There are various steps we can take to simplify the expression in Eq. (54). We first consider the scales μ_H, μ_J, and μ_S. In Sec. V E, we advocated the use of the profile functions in Appendix B to achieve a smooth transition between the different regions of the thrust distribution. Here, we simplify our choice of natural scales to obtain a more illuminating analytic formula:

$$\mu_H = Q, \qquad \mu_J = \sqrt{3\bar{\tau}^c}Q, \qquad \mu_S = 3\bar{\tau}^c Q. \qquad (55)$$

This choice has still the effect of turning off the resummation at $\bar{\tau}^c = 1/3$.

Second, we can simplify the dependence on the two quark track functions. Defining

$$q^L(\mu) \equiv \int dx_A dx_B T_q(x_A, \mu) T_q(x_B, \mu) \ln\left(\frac{x_A + x_B}{2}\right), \qquad (56)$$

it is helpful to use the approximation

$$\int dx_A dx_B T_q(x_A) T_q(x_B) \left(\frac{x_A + x_B}{2}\right)^{\eta_{\bar{s}}} \approx \exp\left(q^L \eta_{\bar{s}}\right). \quad (57)$$

This is formally justified only for $\eta_{\bar{s}} \ll 1$, but for the (PYTHIA-based) track functions, the error is only a few percent even for $\eta_{\bar{s}} = 1$. By contrast, using a linear (as opposed to exponential) approximation in Eq. (57) would yield a $\simeq 20\%$ error at $\eta_{\bar{s}} = 1$.

Finally, because the only difference between the NLL evolution kernels for calorimeter thrust and track thrust appears in the noncusp anomalous dimensions, we can write the track thrust cumulative $\bar{\Sigma}$ in terms of the calorimeter thrust cumulative Σ as

$$\bar{\Sigma}(\bar{\tau}^c) = \Sigma(\bar{\tau}^c) \exp\left(K_{\bar{S}} - K_S\right) \exp\left(q^L \eta_{\bar{S}}\right). \quad (58)$$

From Eq. (A5), we find that the difference between $K_{\bar{S}}$ and K_S is

$$K_{\bar{S}}(\mu_S, \mu_J) - K_S(\mu_S, \mu_J) = \frac{8 C_F g_1^L}{\beta_0} \ln \frac{\alpha_s(\mu_J)}{\alpha_s(\mu_S)}$$
$$\approx \frac{4 \alpha_s C_F}{\pi} g_1^L \ln \frac{\mu_S}{\mu_J}$$
$$= \frac{2 \alpha_s C_F}{\pi} g_1^L \ln (3\bar{\tau}^c). \quad (59)$$

Here we used the running of α_s to obtain the second line, and inserted the natural scales from Eq. (55) in the last step. (Since we only kept the leading term in α_s, different choices for the scale of α_s correspond to effects beyond the order we are working.) Similarly, we find that $\eta_{\bar{S}}$ is given by

$$\eta_{\bar{S}}(\mu_S, \mu_J) = -\frac{8 C_F}{\beta_0} \ln \frac{\alpha_s(\mu_J)}{\alpha_s(\mu_S)} \approx -\frac{2 \alpha_s C_F}{\pi} \ln (3\bar{\tau}^c). \quad (60)$$

This leads to

$$\bar{\Sigma}(\bar{\tau}^c) \approx \Sigma(\bar{\tau}^c) \exp\left[\frac{2 \alpha_s C_F}{\pi} (g_1^L - q^L) \ln (3\bar{\tau}^c)\right], \quad (61)$$

as anticipated in Eq. (6).

Based on Eq. (61), we now have a better understanding of why track thrust and calorimeter thrust are so similar. At NLL order, the difference between the cumulative distributions for track and calorimeter thrust is basically given by an exponential factor. However, this factor depends on g_1^L and q^L, which happen to be nearly equal for the track functions extracted from PYTHIA. For concreteness, we evaluate g_1^L and q^L at the scale $\mu \simeq 20$ GeV, though any choice of scale between μ_S and μ_J is acceptable at this order. We find

$$g_1^L \simeq -0.52, \qquad q^L \in [-0.49, -0.54], \quad (62)$$

where the range corresponds to the variation between different quark flavors. This leads to a cancellation in Eq. (61), which is responsible for the similarity between the calorimeter and track thrust distributions. These parameters have only a mild μ dependence, and the partial cancellation between g_1^L and q^L persists over a wide range of scales.

VII. NUMERICAL RESULTS

With all of the ingredients for the track thrust distribution in place, we now show numerical results as we increase the accuracy of our calculation. In all cases, we show normalized cross sections $(1/\sigma)(d\sigma/d\tau)$, and use our (PYTHIA-based) NLO track functions as input.

In Fig. 8, we show the NLL result from Eq. (54) for calorimeter and track thrust. Here we use the central values for the canonical running scales described in Appendix B. As argued in Sec. VI, the difference between calorimeter and track thrust is very small at NLL order, and is in fact barely visible on this plot.

To achieve NLL′ accuracy, we have to take into account higher-order terms in H, $\bar{J}$, and $\bar{S}$ in Eq. (50), as well as the nonsingular terms from Sec. V F. The result of going from NLL to NLL′ is shown in Fig. 9, which compares the track thrust distributions in the peak and tail regions. The inclusion of the one-loop corrections to the hard, jet, and soft functions at NLL′ reduces the purely perturbative uncertainty bands coming from scale variations. Note that this uncertainty estimate does not include the uncertainty associated with the value of $\alpha_s(M_Z)$ or with the input track functions.
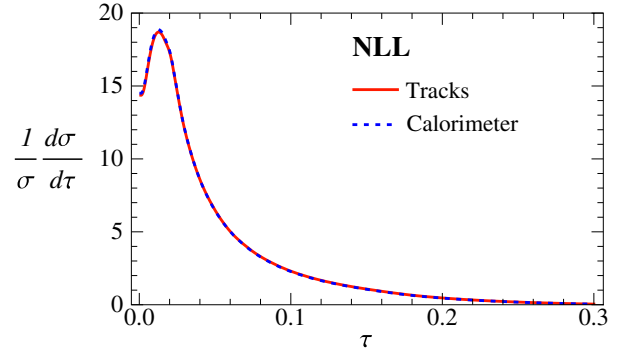
FIG. 8 (color online).   Track thrust and calorimeter thrust at NLL. As explained in Sec. VI, these distributions are remarkably similar.
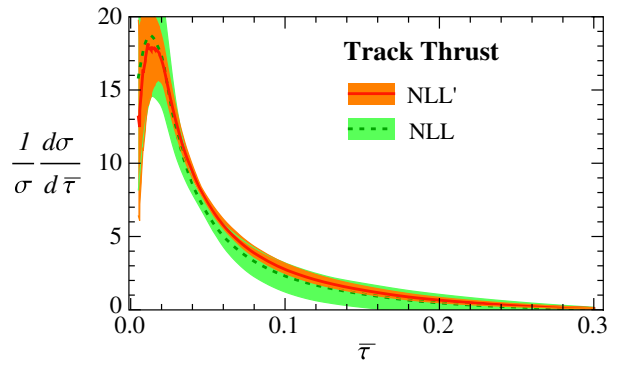
FIG. 9 (color online).   Track thrust distribution going from NLL to NLL′. The bands encode perturbative uncertainties from RG scale variations, but not uncertainties in α_s or the track functions themselves.
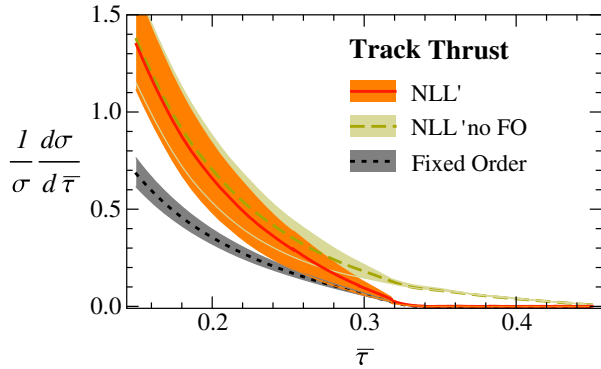
FIG. 10 (color online). Track thrust distribution in the tail and far-tail regions, illustrating the effect of including the nonsingular contribution at NLL′ order. The full NLL′ distribution interpolates between the resummed and fixed-order results.

FIG. 12 (color online). Comparison of analytical predictions with DELPHI data for both track and calorimeter thrust distributions. There is good qualitative and quantitative agreement in the tail region, though as shown in Fig. 3, the theoretical uncertainties at NLL′ are larger than the experimental ones.

The effect of the nonsingular terms on the tail and far-tail regions are highlighted in Fig. 10. The inclusion of these terms guarantees that the cross section merges with the $\mathcal{O}(\alpha_s)$ fixed-order result in the region where the resummation is no longer important. It also ensures that the cross section vanishes beyond the $\mathcal{O}(\alpha_s)$ kinematic endpoint $\tau = 1/3$. (For this to happen, it is crucial that the profile functions in Appendix B turn off the resummation at the endpoint.) As desired, the full NLL′ distribution interpolates between the NLL′ result (without nonsingular terms) at small τ and the fixed-order result at large τ.

In Fig. 11, we augment the NLL′ results with the leading power correction $\bar{\Omega}_1^\tau$. For track thrust, the dominant effect of $\bar{\Omega}_1^\tau$ is a shift, though there are important effects in the peak region which do not amount to a shift. (For the calorimeter thrust distribution, the only effect of Ω_1^τ is to shift the distribution.) Note, however, that the peak region is also sensitive to higher-order power corrections which we have not included. The comparison between calorimeter and track thrust with the leading power correction is shown in Fig. 3.

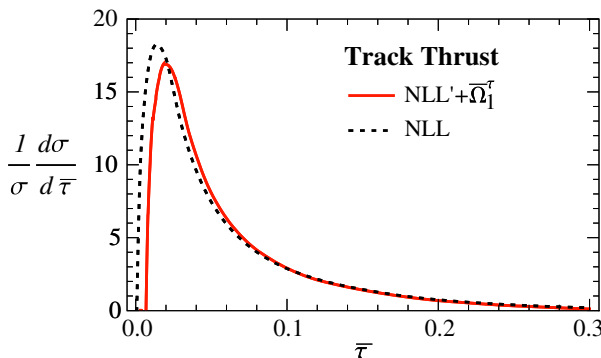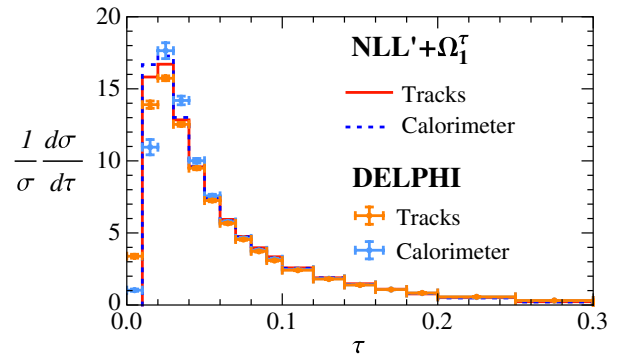In Fig. 12 we superimpose our theoretical predictions for the calorimeter and track thrust distributions with

experimental data from the DELPHI Collaboration. At NLL′ order with the leading power correction $\bar{\Omega}_1^\tau$, the agreement is quite good, though we emphasize that we chose values of α_s and $\bar{\Omega}_1^\tau$ to ensure reasonable agreement with the calorimeter thrust data. We show the effect of scale uncertainties in Fig. 3, which are in general larger than the experimental uncertainties, motivating future studies of track thrust with higher orders of resummation and more accurate fixed-order corrections.

As a final cross check of our analysis, we show the calorimeter and track thrust distributions from PYTHIA in Fig. 13. Since PYTHIA has been tuned to LEP data, it agrees well with the DELPHI measurements. There is good agreement between PYTHIA and our NLL′ result in the tail region, but there are difference in the peak region due to the fact that PYTHIA includes an estimate of the full nonperturbative corrections, whereas we only include the leading power correction. Future track thrust calculations could use a full nonperturbative shape function for better modeling of the $\bar{\tau} \simeq 0$ region.

FIG. 11 (color online). Track thrust at NLL′ adding the leading power correction.
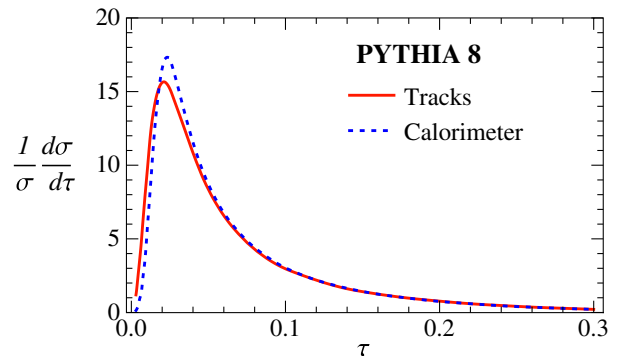

FIG. 13 (color online). Calorimeter and track thrust distributions obtained from PYTHIA 8. Apart from deviations in the peak region due to higher-order nonperturbative corrections, these agree well with our NLL′ calculation after the leading power correction is included (compare to Fig. 3).

VIII. DISCUSSION

In this paper, we have presented the first calculation of track thrust in perturbative QCD. Our result is accurate to $\mathcal{O}(\alpha_s)$ in a fixed-order expansion while also including NLL resummation, i.e. NLL$'$ order. By incorporating both track functions and the leading power correction, we have accounted for the dominant nonperturbative effects that determine the track thrust distribution. Our result is in good agreement with track thrust measurements performed at ALEPH and DELPHI.

One feature seen in the data is a remarkable similarity between the calorimeter thrust and track thrust distributions. At NLL, we traced this feature to a partial cancellation between two nonperturbative parameters—one associated with the gluon track function g_1^L, and one associated with pairs of quark track functions q^L. We conjecture that a similar cancellation should be present in most (if not all) dimensionless track-based observables. This should be relatively straightforward to prove for e^+e^- dijet event shapes with a thrust-like factorization theorem, but is likely to persist for more general track-based observables, including jet shapes relevant for the LHC such as N-subjettiness ratios [50,51] or energy correlation functions ratios [52]. It is worth further study to understand whether this partial cancellation is just an accident or reflects some deeper property of track functions. Crucially, we have seen that neither higher-order terms at NLL$'$ nor the leading power correction qualitatively spoil the similarity.

The track functions were originally designed to describe the energy fraction of a parton carried by tracks (i.e. the large component of the light-cone momentum). Track thrust essentially measures the small component of the light-cone momentum carried by tracks, so it is perhaps surprising that the same track functions can be used in this context. The reason this works is that the track thrust distribution can be thought of as arising from multiple gluon emissions, each of which carries its own track function. Just as multiple emissions can be exponentiated in the case of calorimeter thrust, multiple emissions with track functions can also be exponentiated. In our calculation, this shows up in the fact that the anomalous dimension of the soft and jet functions depend on the logarithmic moment of the gluon track function g_1^L. We are confident that similar techniques could be applied to any track-based observable, as long as the calorimetric version of that observable has a valid factorization theorem. This motivates future experimental and theoretical studies of track-based observables.

ACKNOWLEDGMENTS

APPENDIX A: RESUMMATION

For the NLL$'$ distribution in Eq. (50), we need expressions for the evolution kernels. Apart from the nonperturbative parameter g_1^L, the evolution kernels are the same between calorimeter thrust and track thrust, and governed by the relevant RGEs given in Sec. V.

The RGE for the hard function in Eq. (30) leads to the evolution

$$
\begin{aligned}
H(Q^2, \mu) &= H(Q^2, \mu_0) U_H(Q^2, \mu_0, \mu), \\
U_H(Q^2, \mu_0, \mu) &= e^{K_H(\mu_0, \mu)} \left(\frac{Q^2}{\mu_0^2}\right)^{\eta_H(\mu_0, \mu)}, \\
K_H(\mu_0, \mu) &= -4K_\Gamma(\mu_0, \mu) + K_{\gamma_H}(\mu_0, \mu), \\
\eta_H(\mu_0, \mu) &= 2\eta_\Gamma(\mu_0, \mu),
\end{aligned}
\tag{A1}
$$

where $K_\Gamma(\mu_0, \mu)$, $\eta_\Gamma(\mu_0, \mu)$ and K_γ are given below in Eq. (A4). Similarly, the RGE for the jet function in Eq. (49) leads to the evolution

$$
\begin{aligned}
\bar{J}(\bar{s}, x, \mu) &= \int_0^{\bar{s}} d\bar{s}' U_{\bar{J}}(\bar{s} - \bar{s}', \mu_0, \mu) \bar{J}(\bar{s}', x, \mu_0), \\
U_{\bar{J}}(\bar{s}, \mu_0, \mu) &= \frac{e^{K_{\bar{J}} - \gamma_E \eta_{\bar{J}}}}{\Gamma(1 + \eta_{\bar{J}})} \left[\frac{\eta_{\bar{J}}}{\mu_0^2} \mathcal{L}^{\eta_{\bar{J}}} \left(\frac{\bar{s}}{\mu_0^2}\right) + \delta(\bar{s})\right], \\
K_{\bar{J}}(\mu_0, \mu) &= 4K_\Gamma(\mu_0, \mu) + K_{\gamma_{\bar{J}}}(\mu_0, \mu), \\
\eta_{\bar{J}}(\mu_0, \mu) &= -2\eta_\Gamma(\mu_0, \mu).
\end{aligned}
\tag{A2}
$$

The function $K_{\gamma_{\bar{J}}}$ contains the contribution from the nonperturbative parameter g_1^L to the noncusp anomalous dimension $\gamma_{\bar{J}}[\alpha_s]$. Finally, the RGE for the soft function in Eq. (35) leads to the evolution

$$
\begin{aligned}
\bar{S}(\bar{k}, \mu) &= \int_0^{\bar{k}} d\bar{k}' U_{\bar{S}}(\bar{k} - \bar{k}', \mu_0, \mu) \bar{S}(\bar{k}', \mu_0), \\
U_{\bar{S}}(\bar{k}, \mu_0, \mu) &= \frac{e^{K_{\bar{S}} - \gamma_E \eta_{\bar{S}}}}{\Gamma(1 + \eta_{\bar{S}})} \left[\frac{\eta_{\bar{S}}}{\mu_0} \mathcal{L}^{\eta_{\bar{S}}} \left(\frac{\bar{k}}{\mu_0}\right) + \delta(\bar{k})\right], \\
K_{\bar{S}}(\mu_0, \mu) &= -4K_\Gamma(\mu_0, \mu) + K_{\gamma_{\bar{S}}}(\mu_0, \mu), \\
\eta_{\bar{S}}(\mu_0, \mu) &= 4\eta_\Gamma(\mu_0, \mu).
\end{aligned}
\tag{A3}
$$

Here, $K_{\gamma_{\bar{S}}}$ contains the contribution from g_1^L to $\gamma_{\bar{S}}[\alpha_s]$.

The functions $K_\Gamma(\mu_0, \mu)$, $\eta_\Gamma(\mu_0, \mu)$, and $K_{\gamma_x}(\mu_0, \mu)$ in the above RGE solutions are defined as

$$K_\Gamma^i(\mu_0, \mu) = \int_{\alpha_s(\mu_0)}^{\alpha_s(\mu)} \frac{\mathrm{d}\alpha_s}{\beta(\alpha_s)} \Gamma_{\mathrm{cusp}}^i(\alpha_s) \int_{\alpha_s(\mu_0)}^{\alpha_s} \frac{\mathrm{d}\alpha_s'}{\beta(\alpha_s')},$$

$$\eta_\Gamma^i(\mu_0, \mu) = \int_{\alpha_s(\mu_0)}^{\alpha_s(\mu)} \frac{\mathrm{d}\alpha_s}{\beta(\alpha_s)} \Gamma_{\mathrm{cusp}}^i(\alpha_s), \qquad (A4)$$

$$K_{\gamma_x}(\mu_0, \mu) = \int_{\alpha_s(\mu_0)}^{\alpha_s(\mu)} \frac{\mathrm{d}\alpha_s}{\beta(\alpha_s)} \gamma_x(\alpha_s),$$

and their explicit expressions at NLL order are

$$K_\Gamma(\mu_0, \mu) = -\frac{\Gamma_0}{4\beta_0^2} \left\{ \frac{4\pi}{\alpha_s(\mu_0)} \left(1 - \frac{1}{r} - \ln r\right) \right.$$
$$\left. + \left(\frac{\Gamma_1}{\Gamma_0} - \frac{\beta_1}{\beta_0}\right)(1 - r + \ln r) + \frac{\beta_1}{2\beta_0} \ln^2 r \right\},$$

$$\eta_\Gamma(\mu_0, \mu) = -\frac{\Gamma_0}{2\beta_0} \left[\ln r + \frac{\alpha_s(\mu_0)}{4\pi} \left(\frac{\Gamma_1}{\Gamma_0} - \frac{\beta_1}{\beta_0}\right)(r - 1) \right],$$

$$K_{\gamma_x}(\mu_0, \mu) = -\frac{\gamma_{x,0}}{2\beta_0} \ln r. \qquad (A5)$$

Here $r = \alpha_s(\mu)/\alpha_s(\mu_0)$, and β_i, Γ_i, and $\gamma_{x,i}$ are the coefficients of the β function, the cusp, and the noncusp anomalous dimensions in their α_s expansion,

$$\beta(\alpha_s) = -2\alpha_s \sum_{n=0}^{\infty} \beta_n \left(\frac{\alpha_s}{4\pi}\right)^{n+1},$$

$$\Gamma_{\mathrm{cusp}}(\alpha_s) = \sum_{n=0}^{\infty} \Gamma_n \left(\frac{\alpha_s}{4\pi}\right)^{n+1}, \qquad (A6)$$

$$\gamma_x(\alpha_s) = \sum_{n=0}^{\infty} \gamma_{x,n} \left(\frac{\alpha_s}{4\pi}\right)^{n+1}.$$

At NLL$'$ order, we only need the first two coefficients of $\beta(\alpha_s)$ and $\Gamma_{\mathrm{cusp}}(\alpha_s)$, which are

$$\beta_0 = \frac{11}{3} C_A - \frac{4}{3} T_F n_f,$$

$$\beta_1 = \frac{34}{3} C_A^2 - \left(\frac{20}{3} C_A + 4 C_F\right) T_F n_f,$$

$$\Gamma_0 = 4 C_F, \qquad (A7)$$

$$\Gamma_1 = 4 C_F \left[\left(\frac{67}{9} - \frac{\pi^2}{3}\right) C_A - \frac{20}{9} T_F n_f \right].$$

For the noncusp anomalous dimension $\gamma_x(\alpha_s)$ we only need the first coefficient, given in Eqs. (30), (35), and (49).

APPENDIX B: PROFILE FUNCTIONS

The optimal choice of RG scales depends on the value of τ, so we use profile functions to smoothly interpolate between the small τ and large τ regions.

Our choice of running scales is adopted from Ref. [29] with some modifications:

$$\mu_H = e_H Q,$$

$$\mu_J(\tau) = \left[1 + e_J \theta(\tau_3 - \tau)\left(1 - \frac{\tau}{\tau_3}\right)^2\right] \sqrt{\mu_H \mu_{\mathrm{run}}(\tau, \mu_H)},$$

$$\mu_S(\tau) = \left[1 + e_S \theta(\tau_3 - \tau)\left(1 - \frac{\tau}{\tau_3}\right)^2\right] \mu_{\mathrm{run}}(\tau, \mu_H), \quad (B1)$$

where μ_{run} is given by

$$\mu_{\mathrm{run}}(\tau, \mu) = \begin{cases} \mu_0 + a\tau^2/\tau_1 & \tau \le \tau_1, \\ 2a\tau + b & \tau_1 \le \tau \le \tau_2, \\ \mu - a(\tau - \tau_3)^2/(\tau_3 - \tau_2) & \tau_2 \le \tau \le \tau_3, \\ \mu & \tau > \tau_3, \end{cases}$$

$$a = \frac{\mu_0 - \mu}{\tau_1 - \tau_2 - \tau_3}, \quad b = \frac{\mu\tau_1 - \mu_0(\tau_2 + \tau_3)}{\tau_1 - \tau_2 - \tau_3}. \quad (B2)$$

The expressions for a and b follow from demanding that μ_{run} is continuous and has a continuous derivative. The value of μ_0 determines the scales at $\tau = 0$, while $\tau_{1,2,3}$ determine the transition between the peak, tail, and far-tail regions discussed in Sec. V. For $\tau > \tau_3$, our choice for μ_{run} ensures that the resummation of logarithms of τ turns off.

The parameters for the central curve are

$$e_H = 1, \qquad e_B = e_S = 0, \qquad \mu_0 = 2 \text{ GeV},$$
$$\tau_1 = \frac{2 \text{ GeV}}{Q}, \qquad \tau_2 = 0.15, \qquad \tau_3 = 0.33. \qquad (B3)$$

The scale uncertainty bands are obtained by taking the envelope of the following scale variations:

$$(a) \ e_H = 2^{\pm 1}, \quad e_J = e_S = 0,$$
$$(b) \ e_H = 1, \quad e_J = \pm 0.5, \quad e_S = 0, \qquad (B4)$$
$$(c) \ e_H = 1, \quad e_J = 0, \quad e_S = \pm 0.5.$$

APPENDIX C: PLUS DISTRIBUTIONS

The standard plus distribution for some function $g(x)$ is defined as

$$[\theta(x) g(x)]_+ = \lim_{\beta \to 0} \frac{\mathrm{d}}{\mathrm{d}x} [\theta(x - \beta) G(x)] \qquad (C1)$$

with

$$G(x) = \int_1^x \mathrm{d}x' g(x'). \qquad (C2)$$

This satisfies the boundary condition $\int_0^1 \mathrm{d}x [\theta(x) g(x)]_+ = 0$. The two special cases we need in this paper are

$$\mathcal{L}_n(x) \equiv \left[\frac{\theta(x)\ln^n x}{x} \right]_+$$

$$= \lim_{\beta \to 0} \left[\frac{\theta(x-\beta)\ln^n x}{x} + \delta(x-\beta)\frac{\ln^{n+1}\beta}{n+1} \right],$$

$$\mathcal{L}^\eta(x) \equiv \left[\frac{\theta(x)}{x^{1-\eta}} \right]_+ = \lim_{\beta \to 0} \left[\frac{\theta(x-\beta)}{x^{1-\eta}} + \delta(x-\beta)\frac{x^\eta - 1}{\eta} \right].$$

(C3)

In our calculations, we use the plus distribution identities appearing in Appendix B of Ref. [43]. In particular, we utilize the following rescaling identity for a constant λ:

$$\lambda \mathcal{L}_n(\lambda x) = \frac{\ln^{n+1}(\lambda)}{n+1}\delta(x) + \sum_{k=0}^{n}\binom{n}{k}\ln^{n-k}(\lambda)\mathcal{L}_k(x). \quad \text{(C4)}$$

[1] D. Buskulic *et al.* (ALEPH Collaboration), Z. Phys. C **55,** 209 (1992).
[2] P. Abreu *et al.* (DELPHI Collaboration), Z. Phys. C **73,** 11 (1996).
[3] M. Dasgupta and G. P. Salam, J. Phys. G **30,** R143 (2004).
[4] A. Heister *et al.* (ALEPH Collaboration), Eur. Phys. J. C **35,** 457 (2004).
[5] J. Abdallah *et al.* (DELPHI Collaboration), Eur. Phys. J. C **29,** 285 (2003).
[6] P. Achard *et al.* (L3 Collaboration), Phys. Rep. **399,** 71 (2004).
[7] G. Abbiendi *et al.* (OPAL Collaboration), Eur. Phys. J. C **40,** 287 (2005).
[8] D. Krohn, T. Lin, M. D. Schwartz, and W. J. Waalewijn, Phys. Rev. Lett. **110,** 212001 (2013).
[9] W. J. Waalewijn, Phys. Rev. D **86,** 094030 (2012).
[10] H.-M. Chang, M. Procura, J. Thaler, and W. J. Waalewijn, arXiv:1303.6637.
[11] C. W. Bauer, S. Fleming, and M. E. Luke, Phys. Rev. D **63,** 014006 (2000).
[12] C. W. Bauer, S. Fleming, D. Pirjol, and I. W. Stewart, Phys. Rev. D **63,** 114020 (2001).
[13] C. W. Bauer and I. W. Stewart, Phys. Lett. B **516,** 134 (2001).
[14] C. W. Bauer, D. Pirjol, and I. W. Stewart, Phys. Rev. D **65,** 054022 (2002).
[15] T. Sjöstrand, S. Mrenna, and P. Skands, J. High Energy Phys. 05 (2006) 026.
[16] T. Sjöstrand, S. Mrenna, and P. Skands, Comput. Phys. Commun. **178,** 852 (2008).
[17] E. Farhi, Phys. Rev. Lett. **39,** 1587 (1977).
[18] G. Salam and D. Wicke, J. High Energy Phys. 05 (2001) 061.
[19] V. Mateu, I. W. Stewart, and J. Thaler, Phys. Rev. D **87,** 014025 (2013).
[20] T. Kinoshita, J. Math. Phys. (N.Y.) **3,** 650 (1962).
[21] T. Lee and M. Nauenberg, Phys. Rev. **133,** B1549 (1964).
[22] F. A. Berends and W. Giele, Nucl. Phys. **B306,** 759 (1988).
[23] M. L. Mangano and S. J. Parke, Phys. Rep. **200,** 301 (1991).
[24] D. A. Kosower, Nucl. Phys. **B552,** 319 (1999).
[25] J. C. Collins and D. E. Soper, Nucl. Phys. **B193,** 381 (1981).
[26] J. C. Collins and D. E. Soper, Nucl. Phys. **B194,** 445 (1982).
[27] A. Jain, M. Procura, and W. J. Waalewijn, J. High Energy Phys. 05 (2011) 035.
[28] G. Altarelli and G. Parisi, Nucl. Phys. **B126,** 298 (1977).
[29] R. Abbate, M. Fickinger, A. H. Hoang, V. Mateu, and I. W. Stewart, Phys. Rev. D **83,** 074021 (2011).
[30] S. Catani, L. Trentadue, G. Turnock, and B. R. Webber, Nucl. Phys. **B407,** 3 (1993).
[31] G. P. Korchemsky and G. F. Sterman, Nucl. Phys. **B555,** 335 (1999).
[32] S. Fleming, A. H. Hoang, S. Mantry, and I. W. Stewart, Phys. Rev. D **77,** 074010 (2008).
[33] M. D. Schwartz, Phys. Rev. D **77,** 014026 (2008).
[34] A. V. Manohar, Phys. Rev. D **68,** 114019 (2003).
[35] C. W. Bauer, C. Lee, A. V. Manohar, and M. B. Wise, Phys. Rev. D **70,** 034014 (2004).
[36] S. Fleming, A. H. Hoang, S. Mantry, and I. W. Stewart, Phys. Rev. D **77,** 114003 (2008).
[37] A. V. Manohar and M. B. Wise, Phys. Lett. B **344,** 407 (1995).
[38] B. Webber, Phys. Lett. B **339,** 148 (1994).
[39] G. P. Korchemsky and G. F. Sterman, Nucl. Phys. **B437,** 415 (1995).
[40] Y. L. Dokshitzer and B. Webber, Phys. Lett. B **352,** 451 (1995).
[41] G. Korchemsky and S. Tafat, J. High Energy Phys. 10 (2000) 010.
[42] A. H. Hoang and I. W. Stewart, Phys. Lett. B **660,** 483 (2008).
[43] Z. Ligeti, I. W. Stewart, and F. J. Tackmann, Phys. Rev. D **78,** 114014 (2008).
[44] R. Akhoury and V. I. Zakharov, Phys. Lett. B **357,** 646 (1995).
[45] C. Lee and G. F. Sterman, Phys. Rev. D **75,** 014022 (2007).
[46] X. Liu, Phys. Lett. B **699,** 87 (2011).
[47] M. Procura and I. W. Stewart, Phys. Rev. D **81,** 074009 (2010).
[48] T. Hahn, Comput. Phys. Commun. **168,** 78 (2005).
[49] T. Becher and M. D. Schwartz, J. High Energy Phys. 07 (2008) 034.
[50] J. Thaler and K. Van Tilburg, J. High Energy Phys. 03 (2011) 015.
[51] J. Thaler and K. Van Tilburg, J. High Energy Phys. 02 (2012) 093.
[52] A. J. Larkoski, G. P. Salam, and J. Thaler, J. High Energy Phys. 06 (2013) 108.